Inhomogeneous fluid membranes: Segregation, ordering, and effective rigidity

Roland R. Netz* and P. Pincus
Department of Materials, University of California, Santa Barbara, California 93106-9530
(Received 24 January 1995)

Fluid membranes with spatially varying distributions of bending rigidity and spontaneous curvature are considered, which are applicable to inhomogeneous membranes consisting of different components and membranes with inclusions (such as proteins) or adsorbed colloidal particles. Thermally activated shape fluctuations of the membrane induce rather long-ranged interactions between these inhomogeneities, which are free to diffuse laterally and to organize into spatial structures. As a consequence of these interactions, one finds two ordered phases in addition to the disordered phase in which the inhomogeneities are randomly mixed: a segregated phase, where the inclusions tend to aggregate, and a hexagonal phase, where the inclusions maximize their mutual separation. The phase behavior depends crucially on the lateral correlation length within the membrane. Also, the effective bending rigidity of the membrane is calculated for all different phases; in general, the inhomogeneities in the elastic moduli considered here lead to a characteristic softening of the membrane. These results, which are obtained using perturbation theory, are confirmed by Monte Carlo simulations. Experimental applications comprise proteins or adsorbed colloidal particles in vesicular bilayers and lamellar stacks and membranes consisting of lipid mixtures.

PACS number(s): 82.70.−y, 87.22.Bt, 64.60.−i, 64.75.+g

I. INTRODUCTION

In experimental and biological situations, fluid membranes are usually inhomogeneous on some microscopic length scale. Typically, membranes consist of mixtures of various lipids with in general different elastic properties, or can incorporate larger inclusions (such as proteins) or host adsorbed colloidal particles or other macromolecules, which locally perturb the elastic and structural properties of the pure membrane. The experimentally observed behavior for such mixed systems is very complex and shows phase separation of the different membrane constituents, randomly mixed states, and more complicated modes of aggregation of larger inclusions [1–5]. Apart from direct interactions between the inclusions or the different components making up the membrane, which certainly do exist, there are a number of effects due to the lipid matrix the inclusions are embedded in. On the theoretical side, it was found very early that the presence of a protein in a membrane leads to structural changes in the lipid environment, which in turn give rise to lipid-mediated interactions between two of these inclusions [6]. This was formulated subsequently in terms of Landau theories for an order parameter connected to some local property of the membrane, usually taken to be the degree of chain ordering or the density of lipid molecules [7–9]. Aggregation was also argued to result from a hydrophobic mismatch between proteins and the surrounding membrane [10]. Quite complementarily, the distortion of a membrane around an inclusion was studied using the standard elasticity model of membranes, giving rise to attractive or repulsive interactions between two inclusions, depending on the elastic properties of the two monolayers making up the bilayer [11].

On a more fundamental level, inclusions and other inhomogeneous structures lead to spatially varying elastic properties of the mixed membrane system, according to the distribution and the elastic properties of the different constituents. It has been realized very recently that thermally activated shape fluctuations of the embedding membrane then give rise to interactions between the different components distinguished by their elastic moduli, even without additional coupling between the inclusions and the surrounding membrane [12–14]. Clearly, such interactions are ubiquitous and universal in the sense that they depend only on the coarse-grained elastic moduli of the membrane constituents. In many cases these fluctuation-induced forces will be exceeded by direct interactions between inclusions; however, in the last section we will report on ways to experimentally single out these indirect forces.

In this article, we first derive the shape-fluctuation-induced interaction between inclusions which locally change the (i) bending rigidity and (ii) spontaneous curvature of the membrane. This is done in the harmonic approximation for a finite in-plane correlation length of the membrane. We then calculate the free energy of different lateral arrangements of the inclusions, by summing over all interactions between them, and arrive at a phase diagram, featuring the disordered phase, where the different constituents are randomly mixed, an aggregated phase, where the inclusions phase separate from the pure membrane, and a hexagonal phase, where the (asymmetric) inclusions keep maximal distance from each other. We also calculate the effective elastic properties of the

*Present address: Department of Physics, Box 351560, University of Washington, Seattle, WA 98195-1560.

mixed membrane in each phase; one obtains a characteristic softening due to the coordinated interplay of the membrane shape fluctuations and the distribution of the elastic moduli. These results are obtained using a perturbation scheme, with the differential elastic constants being the small parameter. Monte Carlo simulations performed for a selected set of parameters and for a more realistic interaction potential between membranes containing a hard wall confirm the analytic predictions. At the end, we discuss in detail how these predictions can be checked experimentally. It is also shown how the notion of an effective bending rigidity can be invoked to understand the trend to aggregation for very stiff inclusions.

II. FLUCTUATION-INDUCED FORCES BETWEEN PAIRS OF INCLUSIONS

The effective Hamiltonian of a homogeneous membrane which is on average flat can be written as [15]

$$\mathcal{H}_0 = \int d^2\mathbf{x} \left\{ \frac{1}{2}\kappa_0 \left[\nabla^2 l(\mathbf{x}) - c_0\right]^2 + V(l(\mathbf{x})) \right\}, \quad (1)$$

where κ_0 is the bending-rigidity modulus and c_0 the spontaneous curvature of the membrane. The displacement field $l(\mathbf{x})$ either describes the shape of a single membrane, subject to an external potential $V(l)$, or the separation between two membranes [16], interacting via the mutual potential $V(l)$. In most cases the membrane is up-down symmetric and the spontaneous curvature vanishes. Even if c_0 is nonzero it does not affect a membrane as described by (1) since the integral over the terms depending on c_0 is a constant not depending on the shape of the membrane. The Gaussian curvature is not taken into account; the corresponding elastic constant for membranes and for inclusions as well is not known.

We will now discuss the effect of an inclusion or an adsorbed particle on the elastic properties of a membrane defined by Hamiltonian (1). An inclusion which is stiffer than the embedding membrane constitutes a locus of increased bending rigidity [see Fig. 1(a) for a schematic picture]; in analogy, a tightly bound flat particle will stiffen the membrane locally [see Fig. 1(b)]. In addition, an inclusion can be up-down asymmetric and thus also induce a local spontaneous curvature [see Fig. 1(c)]. For an adsorbed particle the same effect obtains if the adsorbate is rather spherical than plate like [see Fig. 1(d)]. In general, one will encounter a mixture of these two effects. Note that holes in the membrane correspond to regions of decreased bending rigidity [17]. Naturally, the same description holds for mixtures of lipids with different bending rigidities and spontaneous curvatures, though on a much smaller length scale.

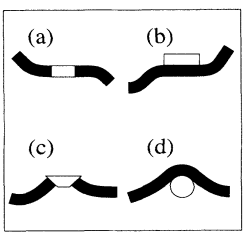

FIG. 1. Schematic picture of (a) an inclusion or (b) an adsorbed macroparticle changing the local bending rigidity, and (c) an inclusion or (d) an adsorbed particle giving rise to a local spontaneous curvature.

To make the above notions concrete, let us consider an inclusion with an area a^2 and bending rigidity of $\kappa_0 + \delta\kappa_\alpha$ and spontaneous curvature of $c_0 + \delta c_\alpha$; clearly, the *bare* perturbation parameters are given by the differential elastic constants $\delta\kappa_\alpha$ and δc_α. The *effective* perturbation parameters turn out to be $\delta\kappa_\alpha/\kappa_0$ and $\delta c_\alpha a\sqrt{\kappa_0/T}$. The energy contribution of an inclusion positioned at $\mathbf{x} = \mathbf{x}_\alpha$ (and neglecting the finite area extent) can be written as

$$\mathcal{H}_\alpha(\mathbf{x}_\alpha) = \frac{1}{2}\delta\kappa_\alpha a^2 \left[\nabla^2 l(\mathbf{x}_\alpha)\right]^2 - \delta c_\alpha \kappa_0 a^2 \nabla^2 l(\mathbf{x}_\alpha). \quad (2)$$

It is a well established fact that the local perturbation of a membrane due to inclusions induces mutual interactions between them [18,12,11]. Here, we derive this interaction for finite temperature and finite correlation length of the membrane, in which case shape fluctuations have to be taken into account. For two inclusions defined by (2) and located at $\mathbf{x} = \mathbf{x}_1$ and $\mathbf{x} = \mathbf{x}_2$, the interaction energy $\mathcal{F}^{(2)}(\mathbf{x}_1 - \mathbf{x}_2)$ can be calculated perturbatively [12,13], noting that

$$\mathcal{F}^{(2)}(\mathbf{x}_1 - \mathbf{x}_2) = -T\ln\left\{ \frac{\int \mathcal{D}l e^{-[\mathcal{H}_0 + \mathcal{H}_1(\mathbf{x}_1) + \mathcal{H}_2(\mathbf{x}_2)]/T}}{\int \mathcal{D}l e^{-\mathcal{H}_0/T}} \right\} - \mathcal{F}_1^{(1)} - \mathcal{F}_2^{(1)}, \quad (3)$$

$$\mathcal{F}_\alpha^{(1)} = -T\ln\left\{ \frac{\int \mathcal{D}l e^{-[\mathcal{H}_0 + \mathcal{H}_\alpha(\mathbf{x}_\alpha)]/T}}{\int \mathcal{D}l e^{-\mathcal{H}_0/T}} \right\}, \quad (4)$$

and is given up to second order in the perturbation parameters by

$$\mathcal{F}^{(2)}(\mathbf{x}_1 - \mathbf{x}_2) = -\frac{a^4\delta\kappa_1\delta\kappa_2}{4T} C^{(4)}_{\nabla^2}(\mathbf{x}_1 - \mathbf{x}_2) - \frac{a^4\kappa_0^2\delta c_1\delta c_2}{T} C^{(2)}_{\nabla^2}(\mathbf{x}_1 - \mathbf{x}_2). \quad (5)$$

$\mathcal{F}^{(1)}$ is the self energy of an inclusion and will be calculated in the next section. Note that at this order of the perturbation theory there is no mixing between the rigidity and the spontaneous-curvature coupling. The two- and four-point correlation functions $C^{(2)}_{\nabla^2}(\mathbf{x})$ and $C^{(4)}_{\nabla^2}(\mathbf{x})$ are known for a harmonic potential $V(l) = (m/2)l^2$ and calculated in Appendix A [13]; both decay exponentially with a characteristic length given by the in-plane correlation length. The bending energy-energy correlation function $C^{(4)}_{\nabla^2}$ is positive for all separations, and the interaction due to the rigidity perturbation is thus attractive if $\delta\kappa_1$ and $\delta\kappa_2$ have the same sign. This attraction can lead to aggregation between inclusions which are much stiffer

than the embedding membrane, as will be calculated in the next section. The curvature-curvature correlation function $C^{(2)}_{\nabla^2}$ is actually repulsive for small distances and oscillates for distances large compared to the membrane in-plane correlation length. This behavior is also obtained for more realistic potentials $V(l)$ taking into account the impenetrability of neighboring membranes [19]. The interaction due to the spontaneous curvature perturbation thus is predominantly repulsive if δc_1 and δc_2 have the same sign. As will be shown in the next section, this short-range repulsion can lead to modulated (hexagonal) ordering of the inclusions, if the spontaneous curvatures of the inclusions are all oriented in one direction.

III. EXTENDED PHASES

In this section we calculate the free energy of different ordered phases up to second order in the perturbation parameters $\delta\kappa$ and δc. This corresponds to an accurate summation of all pair interactions, neglecting higher multibody interactions. For the calculation of the free energy of ordered phases it is instructive to compute first the self energy of an inclusion, defined by (2) and (4). Up to second order it is given by

$$\mathcal{F}^{(1)}_\alpha = \left(\frac{a^2\delta\kappa_\alpha}{2} - \frac{a^4\kappa_0^2\delta c_\alpha^2}{2T}\right)\int_{\mathbf{q}} \mathbf{q}^4 G^{(2)}(\mathbf{q}) - \frac{a^4\delta\kappa_\alpha^2}{4T}\left[\int_{\mathbf{q}} \mathbf{q}^4 G^{(2)}(\mathbf{q})\right]^2 , \tag{6}$$

where the propagator for Hamiltonian (1) in the harmonic approximation defined by $V(l) = (m/2)l^2$ is $G^{(2)}(\mathbf{q}) = T/(\kappa_0\mathbf{q}^4 + m)$. For adsorbed particles, the self energy $\mathcal{F}^{(1)}$ contributes to the adsorption energy, thus influencing the mean coverage of particles if there is equilibrium between adsorbed particles and particles immersed in the intervening solvent. It is noted that the self energy connected to the spontaneous curvature of the inclusions is always negative, thus enhancing the adsorption of spherical particles from the solution.

In the following we calculate the free energy of different distributions of inclusions; the perturbation Hamiltonian $\mathcal{H}'$ now involves an integration over the reference plane and can be written as

$$\mathcal{H}' = \int d^2\mathbf{x}\left\{\frac{1}{2}\delta\kappa(\mathbf{x})\left[\nabla^2 l(\mathbf{x})\right]^2 - \kappa_0\delta c(\mathbf{x})\nabla^2 l(\mathbf{x})\right\}. \tag{7}$$

The free energy per unit area for given distributions $\delta\kappa(\mathbf{x})$ and $\delta c(\mathbf{x})$ then reads

$$f = -\frac{T}{A}\ln\left\{\frac{\int \mathcal{D}l e^{-(\mathcal{H}_0+\mathcal{H}')/T}}{\int \mathcal{D}l e^{-\mathcal{H}_0/T}}\right\}, \tag{8}$$

where A is the total area defined by $\int d^2\mathbf{x} = A$.

The simplest phase is the condensed phase with homogeneous coverage of the inclusions, where $\delta\kappa(\mathbf{x}) = \delta\kappa$ and $\delta c(\mathbf{x}) = \delta c$, assuming that the inclusions are all oriented. The free energy per unit area according to (8) is given by (these and other integrals are calculated in Appendix B)

$$f^C = \frac{\delta\kappa}{2}\int_{\mathbf{q}} \mathbf{q}^4 G^{(2)}(\mathbf{q}) - \frac{\delta\kappa^2}{4T}\int_{\mathbf{q}} \mathbf{q}^8\left[G^{(2)}(\mathbf{q})\right]^2. \tag{9}$$

One notes that the spontaneous curvature gives no contribution to the total free energy, which reflects the fact that the integral of the corresponding interaction energy (5) over an infinite domain in fact vanishes. The free energy of the aggregated state of a membrane with a protein area fraction of ϕ, corresponding to a phase separation into a pure membrane domain and a domain close packed with inclusions, is simply $\Delta f^A = \phi f^C - \phi\mathcal{F}^{(1)}/a^2$, where the self energy of the protein has been subtracted, and is given by

$$\Delta f^A = -\frac{\phi\delta\kappa^2}{4T}\left[\int_{\mathbf{q}} \mathbf{q}^8\left[G^{(2)}(\mathbf{q})\right]^2 - a^2\left[\int_{\mathbf{q}} \mathbf{q}^4 G^{(2)}(\mathbf{q})\right]^2\right] + \frac{\phi a^2\kappa_0^2\delta c^2}{2T}\int_{\mathbf{q}} \mathbf{q}^4 G^{(2)}(\mathbf{q}). \tag{10}$$

In the disordered phase, the distributions $\delta\kappa(\mathbf{x})$ and $\delta c(\mathbf{x})$ are conveniently defined via their moments which for an uncorrelated bimodal distribution take the values

$$\overline{\delta\kappa(\mathbf{x})} = \phi\delta\kappa , \tag{11}$$

$$\overline{\delta c(\mathbf{x})} = \phi\delta c , \tag{12}$$

$$\overline{\delta\kappa(\mathbf{x})\delta\kappa(\mathbf{y})} = \begin{cases} \phi^2\delta\kappa^2 & \text{for } \mathbf{x}\neq\mathbf{y} \\ \phi\delta\kappa^2 & \text{for } \mathbf{x}=\mathbf{y}, \end{cases} \tag{13}$$

$$\overline{\delta c(\mathbf{x})\delta c(\mathbf{y})} = \begin{cases} \phi^2\delta c^2 & \text{for } \mathbf{x}\neq\mathbf{y} \\ \phi\delta c^2 & \text{for } \mathbf{x}=\mathbf{y}, \end{cases} \tag{14}$$

where the overbar denotes an average over all distribution functions $\delta\kappa(\mathbf{x})$ and $\delta c(\mathbf{x})$. For the following results, the averaging over the disorder was done after taking the logarithm in Eq. (8), corresponding to a quenched disordered distribution of inclusions. This amounts to neglecting correlations between the inclusions in the disordered phase [20]. In the same spirit, one can use a random-mixing approximation for the entropic contribution, and the free energy density for the disordered phase turns out to be

$$\Delta f^D = \phi\Delta f^A + T\{\phi\ln(\phi) + (1-\phi)\ln(1-\phi)/a^2\}. \tag{15}$$

As was pointed out in Sec. II, the spontaneous-curvature-induced interaction is repulsive at short distances and thus favors ordered structures where the oriented inclusions maximize the distance from each other; we therefore calculated the free energies of various modulated phases. Such phases (but not the aggregated phase) have also been obtained for inclusions the spontaneous curvatures of which obey a Gaussian probability distribution, in which case the functional integral over the inclusion

configurations can be performed exactly without resorting to a perturbation analysis [21,22].

For the representation of hexagonal ordering we define the function

$$\begin{aligned}\psi(\mathbf{x}) &\equiv \cos(\mathbf{Q}_1\cdot\mathbf{x})\cos(\mathbf{Q}_2\cdot\mathbf{x})\cos(\mathbf{Q}_3\cdot\mathbf{x}) \\ &= [\cos(2\mathbf{Q}_1\cdot\mathbf{x})+\cos(2\mathbf{Q}_2\cdot\mathbf{x}) \\ &\quad +\cos(2\mathbf{Q}_3\cdot\mathbf{x})]/4+1/4, \end{aligned} \tag{16}$$

where $\mathbf{Q}_1 = Q(0,2/\sqrt{3})$, $\mathbf{Q}_2 = Q(1,1/\sqrt{3})$, $\mathbf{Q}_3 = Q(-1,1/\sqrt{3})$, and $Q = 2\pi/d$ with d being the distance between nearest neighbors in the hexagonal array. In order to take into account the discrete nature of the spatial distribution of inclusions, the function $\psi(\mathbf{x})$, which varies between 0 and 1, is taken to represent the probability distribution of finding a protein at position $\mathbf{x}$. In analogy to the disordered phase, the distributions $\delta\kappa(\mathbf{x})$ and $\delta c(\mathbf{x})$ are then defined via their first moments

$$\overline{\delta\kappa(\mathbf{x})} = \psi(\mathbf{x})\delta\kappa\ , \tag{17}$$

$$\overline{\delta c(\mathbf{x})} = \psi(\mathbf{x})\delta c\ , \tag{18}$$

$$\overline{\delta\kappa(\mathbf{x})\delta\kappa(\mathbf{y})} = \begin{cases} \psi(\mathbf{x})\psi(\mathbf{y})\delta\kappa^2 & \text{for } \mathbf{x}\neq\mathbf{y} \\ \psi(\mathbf{x})\delta\kappa^2 & \text{for } \mathbf{x}=\mathbf{y}, \end{cases} \tag{19}$$

$$\overline{\delta c(\mathbf{x})\delta c(\mathbf{y})} = \begin{cases} \psi(\mathbf{x})\psi(\mathbf{y})\delta c^2 & \text{for } \mathbf{x}\neq\mathbf{y} \\ \psi(\mathbf{x})\delta c^2 & \text{for } \mathbf{x}=\mathbf{y}. \end{cases} \tag{20}$$

In the single-mode approximation used here, the inclusion density is fixed at $\phi = \int_{\mathbf{x}} d\mathbf{x}\psi(\mathbf{x})/A = 1/4$; for the density to be an independent parameter one would actually have to go beyond single-mode approximation, which is not attempted here. At this level of the theory, for a density $\phi < 1/4$ the hexagonal phase can be thought of as composed of two regions with $\phi = 1/4$ and $\phi = 0$, respectively.

The free energy of the hexagonal phase of oriented inclusions is then given by

$$\begin{aligned}\Delta f^H = &-\frac{\phi\delta\kappa^2}{32T}\left\{2\int_{\mathbf{q}}\mathbf{q}^8\left[G^{(2)}(\mathbf{q})\right]^2+3\int_{\mathbf{q}}\mathbf{q}^4G^{(2)}(\mathbf{q})(2\mathbf{Q}_1+\mathbf{q})^4G^{(2)}(2\mathbf{Q}_1+\mathbf{q})-5a^2\left[\int_{\mathbf{q}}\mathbf{q}^4G^{(2)}(\mathbf{q})\right]^2\right\} \\ &+\frac{\phi a^2\kappa_0^2\delta c^2}{16T}\left\{5\int_{\mathbf{q}}\mathbf{q}^4G^{(2)}(\mathbf{q})-3(2\mathbf{Q}_1)^4G^{(2)}(2\mathbf{Q}_1)\right\}. \end{aligned} \tag{21}$$

The various integrals appearing in the free-energy expressions are calculated in Appendix B. Other modulated structures, such as striped or chessboard phases, have also been considered but at most coexist with the hexagonal phase, as will be discussed further below. With the reduced parameters $\hat{\xi}_{\|} \equiv \xi_{\|}/a$, $\hat{\omega} \equiv 16\kappa_0^3\delta c^2a^2\hat{\xi}_{\|}^2/T\delta\kappa^2$, $\hat{S} = 128\kappa_0^2/\delta\kappa^2$, $\hat{Q} = 2Q\xi_{\|}\sqrt{2/3}$, and using the in-plane correlation length $\xi_{\|} \equiv (4\kappa_0/m)^{1/4}$, the reduced free energies of all relevant phases can be written as

$$\Delta\hat{f}^A = -4\left(1-\frac{1}{2\hat{\xi}_{\|}^2}\right)+4\hat{\omega}\left(1-\frac{1}{4\hat{\xi}_{\|}^2}\right), \tag{22}$$

$$\Delta\hat{f}^D = \phi\Delta\hat{f}^A+\hat{\xi}_{\|}^2\hat{S}\{\phi\ln(\phi)+(1-\phi)\ln(1-\phi)\}/\phi\ , \tag{23}$$

$$\begin{aligned}\Delta\hat{f}^H = &-\left(1-\frac{5}{4\hat{\xi}_{\|}^2}+\frac{3}{2}K(\hat{Q})\right) \\ &+\hat{\omega}\left(1+\frac{3}{2}\frac{1}{1+\hat{Q}^4}-\frac{5}{8\hat{\xi}_{\|}^2}\right). \end{aligned} \tag{24}$$

The function $K(\hat{Q})$, which is related to the four-point propagator $G^{(4)}(\mathbf{q}) \equiv 2\int_{\mathbf{p}}G^{(2)}(\mathbf{p}+\mathbf{q})G^{(2)}(\mathbf{p})$, is calculated in Appendix C. A salient feature of the free energies is that they do not depend on the temperature for $\hat{\omega} = 0$. The phase diagram resulting from a minimization of the free energies with an area fraction of the inclusions fixed at $\phi = 1/4$ is shown in Fig. 2(a) for three different values of the parameter $\hat{S}$, namely, $\hat{S} = 0.044$, $\hat{S} = 0.22$, and $\hat{S} = 0.44$, from the outer phase boundaries to the inner ones. The parameter $\hat{\omega}$ measures the asymmetry of the inclusions and is zero for completely symmetric inclusions; for inclusions which are free to flip and change their orientation, the hexagonal phase is never observed since nearest-neighbor pairs will try to minimize their mutual interactions by forming energetically favored antiparallel close-packed pairs. The aggregated phase will thus be stabilized further, but with subtle consequences due to the inherent frustration effects arising for hexagonal close packing of the antialigned pairs of inclusions [23]. For the values of $\hat{S}$ shown here, the aggregated phase (A) and the hexagonal phase (H) are separated by the disordered phase (D). For values smaller than $\hat{S} \approx 0.02$ the aggregated and the hexagonal phases actually meet. For general ϕ and $\hat{S}$, the aggregated phase only occurs for $\hat{\omega} < 1$; in contrast, the hexagonal phase (and other modulated phases as well) is restricted to $\hat{\omega} \geq 0.646$ due to an inherent small-wavelength instability of the free-energy expression (24). As one can see from Fig. 2(a), the aggregated phase vanishes both for very small and for large correlation length.

Such a reentrant behavior can be understood by realizing that the interaction due to the increased rigidity of inclusions, the first term in (5), behaves for large separation as $\mathcal{F}(x) \sim -Ta^4(\delta\kappa/\kappa_0)^2\xi_\parallel^{-3}e^{-2x/\xi_\parallel}/x$, as follows from (A8) and (A12). Clearly, there is a competition due to the $\xi_\parallel$ dependence of the range and the magnitude of the interaction, leading to a maximal attractive interaction for finite correlation length. The interaction due to the spontaneous curvature coupling is asymptotically given by $\mathcal{F}(x) \sim \kappa_0\delta c^2a^4\xi_\parallel^{-3/2}e^{-x/\xi_\parallel}/\sqrt{x}$ and in addition oscillates. The two-dimensional integral over x is in fact scale independent of $\xi_\parallel$, and the hexagonal phase, which is stabilized by the latter interaction, extends down to zero correlation length. We note that scans changing the in-plane correlation length $\xi_\parallel$, which in experiments on lamellar stacks can be easily achieved by changing the mean separation between the membranes, correspond to straight lines passing through the origin.

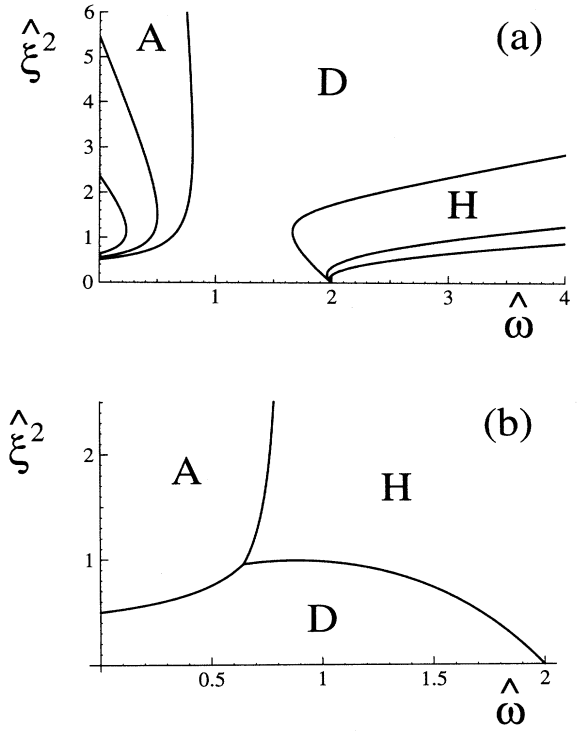

FIG. 2. Phase diagram for fixed inclusion area fraction $\phi = 1/4$ as a function of the rescaled in-plane correlation length $\hat{\xi}_\parallel^2 \equiv \xi_\parallel^2/a^2$ and the ratio of the spontaneous-curvature perturbation and the rigidity perturbation, $\hat{\omega} \equiv 16\kappa_0^3\delta c^2a^2\hat{\xi}_\parallel^2/T\delta\kappa^2$, featuring the disordered phase (D), the aggregated phase (A), and the hexagonal phase (H). Scans of the correlation length correspond to straight lines going through the origin. (a) Shown are results for three different values of the parameter $\hat{S} = 128\kappa_0^2/\delta\kappa^2$, namely, $\hat{S} = 0.044$, $\hat{S} = 0.22$, and $\hat{S} = 0.44$, from the outer phase boundaries to the inner ones. (b) Results for $\hat{S} = 0.0$. The disordered phase has disappeared at large values of $\hat{\xi}_\parallel^2$. On the transition line between the aggregated (A) and the hexagonal (H) phase the stripe phase has identical free energy; on the point where the disordered, hexagonal and aggregated phases coexist, the stripe and the chessboard phase are stable in addition.

Figure 2(b) shows the limiting phase behavior for $\phi = 1/4$ and $\hat{S} = 0$; the disordered phase is only stable for small values of the rescaled correlation length. On the boundary between the hexagonal and aggregated phases, which is independent of the parameters $\hat{S}$ and ϕ and reaches $\hat{\xi}_\parallel^2 = \infty$ for $\hat{\omega} \simeq 0.86$, the striped phase coexists in addition to the two phases meeting there. The striped phase is defined by $\psi(\mathbf{x}) \equiv [1 - \cos(\mathbf{Q}\cdot\mathbf{x})]/2$ with $\mathbf{Q} = Q(0,1)$ and again $Q = 2\pi/d$ (with d being the distance between two neighboring stripes), leading to $\hat{Q} = Q\xi_\parallel/\sqrt{2}$. On the point where all three phases meet, located at $\hat{\omega} = 0.646$ and $\hat{\xi}_\parallel^2 = 0.956\,22$, the chessboard phases coexists with the disordered, the aggregated, and the stripe phases. The chessboard phase is defined by $\psi(\mathbf{x}) \equiv [2 - \cos(\mathbf{Q}_1\cdot\mathbf{x}) - \cos(\mathbf{Q}_2\cdot\mathbf{x})]/4$ with $\mathbf{Q}_1 = Q(0,\sqrt{2})$, $\mathbf{Q}_2 = Q(\sqrt{2},0)$, and $Q = 2\pi/d$, leading to $\hat{Q} = Q\xi_\parallel$. It is quite possible that multibody interactions (which have been neglected here) or direct forces between the inclusions stabilize the stripe or the chessboard phase, leading to a finite phase region between the hexagonal and the aggregated phase where one of these phases could be stable.

In Fig. 3 the phase diagram for $\hat{\omega} = 0$, corresponding to symmetric inclusions, and general ϕ is shown. The values of $\hat{S}$ are $\hat{S} = 0.66$, 0.44, and 0.22, from the inner to the outer phase boundaries. For the limiting value $\hat{S} = 0$ the order extends all the way from $\hat{\xi}_\parallel^2 = 1/2$, the lower bound, to $\hat{\xi}_\parallel^2 = \infty$. For $\hat{S} > 0.72$ there is no order at all. The three circles denote the parameters for which Monte Carlo simulations have been performed. Note that the overall phase diagram is symmetric around $\phi = 1/2$, which reflects the invariance of the condition for coexistence of the aggregated and disordered phases, $\Delta\hat{f}^D - \Delta\hat{f}^A = 0$, under the operation $\phi \to 1 - \phi$.

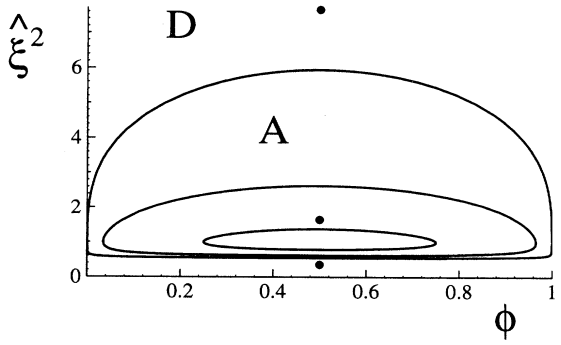

FIG. 3. Phase diagrams for symmetric inclusions ($\hat{\omega} = 0$) as a function of the rescaled in-plane correlation length $\hat{\xi}_\parallel^2$ and the inclusion area fraction ϕ. The values of $\hat{S}$ are $\hat{S} = 0.66$, 0.44, and 0.22, from the inner to the outer phase boundaries. The circles denote parameter values for which Monte Carlo simulations have been performed.

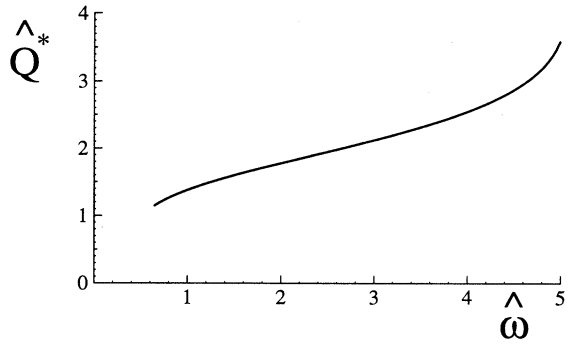

FIG. 4. Plot of the wave vector $\hat{Q}^*$ which minimizes the function $\Omega(\hat{Q}) \equiv \hat{\omega}/(1+\hat{Q}^4) - K(\hat{Q})$ as a function of $\hat{\omega}$. For $\hat{\omega} < 0.646$ one obtains $\hat{Q}^* = 0$. For $\hat{\omega} > 5$, on the other hand, one obtains $\hat{Q}^* = \infty$ and $\Omega(\hat{Q}^*) = 0$.

In the perturbation calculation, the linear size of an inclusion a was taken to coincide with the small-scale cutoff $a_\parallel$ of the underlying lipid matrix; in practice, one expects the two different length scales to enter the free energies. The entropy of mixing will scale as $\sim a_\parallel^2/a^2$; the remaining energetic contributions are expected to scale as $\sim a_\parallel/a$ in the limit $\xi_\parallel \ll a/\sqrt{\phi}$, when all interactions are of sufficiently short range. It follows that the parameter $\hat{S}$ should in fact scale as $\sim a_\parallel/a$; as follows from the phase diagrams in Fig. 2 ordering should thus be facilitated with increasing size of the inclusions, as indeed demonstrated by the Monte Carlo simulations; see Sec. V.

The phase diagram in Fig. 2 results after minimization of the free energy of the hexagonal phase (and the other modulated phases considered) with respect to the wave vector $\hat{Q}$. This entails minimizing the function $\Omega(\hat{Q}) \equiv \hat{\omega}/(1+\hat{Q}^4) - K(\hat{Q})$, leading to the minimizing value $\hat{Q}^*$ which is plotted in Fig. 4 as a function of $\hat{\omega}$. For $\hat{\omega} < 0.646$ one obtains $\hat{Q}^* = 0$, which leads to the aforementioned instability of modulated phases with respect to aggregation; for $\hat{\omega} > 5$, on the other hand, one obtains $\hat{Q}^* = \infty$ and $\Omega(\hat{Q}^*) = 0$.

IV. EFFECTIVE RIGIDITY

In this section we use perturbation theory to estimate the effective bending rigidity of an inhomogeneous membrane, which may be defined via the roughness in the following way: For a homogeneous membrane defined by the Hamiltonian (1), the roughness is given by

$$\langle l^2\rangle_0 = \int_{\mathbf{q}} G^{(2)}(\mathbf{q}) = \frac{T}{8\sqrt{\kappa_0 m}}. \tag{25}$$

In analogy, the effective rigidity κ_{eff} for an inhomogeneous membrane characterized by an additional perturbation $\mathcal{H}'$ as given by (7) may be defined in a heuristic manner by

$$\langle l^2\rangle = \frac{\int \mathcal{D}l\ l^2 e^{-(\mathcal{H}_0+\mathcal{H}')/T}}{\int \mathcal{D}l e^{-(\mathcal{H}_0+\mathcal{H}')/T}} \equiv \frac{T}{8\sqrt{\kappa_{eff} m}}. \tag{26}$$

In the following, we present results up to second order in the rigidity and the spontaneous-curvature perturbation; this is done separately, since there is no mixing between the two perturbations at this order. For the extended phases, Sec. IV A 2, we will again present results for quenched averages over the inclusion distribution; in Sec. IV A 3 we extend the discussion to annealed averages as well and show that the two ensembles are in fact equivalent for a fixed density ϕ of inclusions.

A. Rigidity inhomogeneity

1. Single inclusion

We first consider the effect of a single inclusion defined by the Hamiltonian (2) and located at $\mathbf{x}_1 = \mathbf{0}$. The roughness at a position $\mathbf{x}$ then turns out to be

$$\begin{aligned}\langle l(\mathbf{x})^2\rangle &= \langle l^2\rangle_0 - \frac{a^2\delta\kappa}{2T}\langle l(\mathbf{x})^2[\nabla^2 l(\mathbf{0})^2]^2\rangle_0^c + \frac{a^4\delta\kappa^2}{8T^2}\langle l(\mathbf{x})^2[\nabla^2 l(\mathbf{0})^2]^4\rangle_0^c \\ &= \langle l^2\rangle_0 - \frac{a^2\delta\kappa}{T}[C_\nabla^{(2)}(\mathbf{x})]^2 + \frac{a^4\delta\kappa^2}{T^2}C_{\nabla^2}^{(2)}(\mathbf{0})[C_\nabla^{(2)}(\mathbf{x})]^2,\end{aligned} \tag{27}$$

where the correlation function $C_\nabla^{(2)}(\mathbf{x})$ is defined and calculated in Appendix A. For $\mathbf{x} = \mathbf{0}$, right at the location of the inclusion itself, the roughness is given by

$$\langle l(\mathbf{0})^2\rangle = \langle l^2\rangle_0\left\{1 - \frac{4\delta\kappa}{\kappa_0\hat{\xi}_\parallel^2}\left[\ln(\hat{\xi}_\parallel^4/4+1)\right]^2 \times\left(1-\frac{\delta\kappa}{\kappa_0}(1-1/4\hat{\xi}_\parallel^2)\right)\right\} \tag{28}$$

as follows from the integrals given in Appendix B. For $\mathbf{x} \neq \mathbf{0}$ the roughness is

$$\langle l(\mathbf{x})^2\rangle = \langle l^2\rangle_0\left\{1 - \frac{4\delta\kappa}{\pi^2\kappa_0\hat{\xi}_\parallel^2}\left[\ker(\sqrt{2}x/\xi_\parallel)\right]^2 \times\left(1-\frac{\delta\kappa}{\kappa_0}(1-1/4\hat{\xi}_\parallel^2)\right)\right\}. \tag{29}$$

Asymptotically, for $\hat{\xi}_{\|} \to \infty$, the effect of an inclusion on the roughness at its location vanishes; as a function of the distance from the inclusion, there is an additional exponential damping with distance which comes from the Thomson function [24].

2. *Extended phases*

In general, the roughness of an inhomogeneous membrane defined by Hamiltonian (1) and a perturbation (7) for a quenched distribution of bending rigidities is given by

$$\langle l^2 \rangle = \langle l^2 \rangle_0 - \frac{1}{2AT} \int_{\mathbf{xy}} \overline{\delta\kappa(\mathbf{y})} \langle l(\mathbf{x})^2 [\nabla^2 l(\mathbf{y})]^2 \rangle_0^c + \frac{1}{A8T^2} \int_{\mathbf{xyz}} \overline{\delta\kappa(\mathbf{y})\delta\kappa(\mathbf{z})} \langle l(\mathbf{x})^2 [\nabla^2 l(\mathbf{y})]^2 \times [\nabla^2 l(\mathbf{z})]^2 \rangle_0^c \, . \tag{30}$$

As a check, we first calculate the roughness for the case of homogeneous coverage with inclusions, the condensed phase, defined by $\delta\kappa(\mathbf{x}) = \delta\kappa$. One obtains

$$\langle l^2 \rangle^C = \langle l^2 \rangle_0 - \frac{\delta\kappa}{T} \int_{\mathbf{q}} \mathbf{q}^4 \left[G^{(2)}(\mathbf{q}) \right]^2 + \frac{\delta\kappa^2}{T^2} \int_{\mathbf{q}} \mathbf{q}^8 \left[G^{(2)}(\mathbf{q}) \right]^3 , \tag{31}$$

leading to

$$\langle l^2 \rangle^C = \langle l^2 \rangle_0 \left\{ 1 - \frac{\delta\kappa}{2\kappa_0} + \frac{3\delta\kappa^2}{8\kappa_0^2} \right\} , \tag{32}$$

which corresponds to the first terms of a perturbative expansion of (26) with $\kappa_{eff} = \kappa_0 + \delta\kappa$, just as one would expect.

For the disordered phase with a coverage of ϕ, defined by (11) and (13), one obtains

$$\langle l^2 \rangle^D = \langle l^2 \rangle_0 - \frac{\phi\delta\kappa}{T} \int_{\mathbf{q}} \mathbf{q}^4 \left[G^{(2)}(\mathbf{q}) \right]^2 + \frac{\phi^2\delta\kappa^2}{T^2} \int_{\mathbf{q}} \mathbf{q}^8 \left[G^{(2)}(\mathbf{q}) \right]^3 + \frac{(\phi - \phi^2)\delta\kappa^2 a^2}{T^2} \int_{\mathbf{q}} \mathbf{q}^4 \left[G^{(2)}(\mathbf{q}) \right]^2 \int_{\mathbf{p}} \mathbf{p}^4 G^{(2)}(\mathbf{p})$$
$$= \langle l^2 \rangle_0 \left\{ 1 - \frac{\phi\delta\kappa}{2\kappa_0} + \frac{3\phi^2\delta\kappa^2}{8\kappa_0^2} + (\phi - \phi^2)\frac{\delta\kappa^2}{2\kappa_0^2}(1 - 1/4\hat{\xi}_{\|}^2) \right\} , \tag{33}$$

where all integrals are given in Appendix B. By comparison with (26), the effective rigidity turns out to be given by

$$\kappa_{eff} = \kappa_0 \left\{ 1 + \phi\frac{\delta\kappa}{\kappa_0} - (\phi - \phi^2)\frac{\delta\kappa^2}{\kappa_0^2}(1 - 1/4\hat{\xi}_{\|}^2) \right\} . \tag{34}$$

For $\hat{\xi}_{\|} \gg 1$ this result can be written in the intuitively more appealing form

$$\frac{1}{\kappa_{eff}} = \frac{1-\phi}{\kappa_0} + \frac{\phi}{\kappa_0 + \delta\kappa} . \tag{35}$$

Asymptotically, the effective rigidity κ_{eff} is given by the harmonic average of the rigidities of the pure membrane, κ_0, and the perturbed membrane, $\kappa_0 + \delta\kappa$, weighted with the respective area fraction, and is thus considerably smaller than the arithmetic average, defined by $\overline{\kappa} \equiv (1-\phi)\kappa_0 + \phi(\kappa_0 + \delta\kappa)$. The arithmetically averaged bending rigidity $\overline{\kappa}$ applies to macroscopic deformations with prescribed bending shape [27]. The softening of the membrane as described by the difference $\overline{\kappa} - \kappa_{eff}$ is due to a coupling of shape fluctuations of the membrane to the lateral distribution of bending rigidities. Softening of a membrane has also been observed in the context of inhomogeneous polymeric surfactant interfaces (mixed brushes) [29] and adsorbed polymers [30]. A formula similar to (35) has been proposed earlier on rather general grounds [28,25]. The present treatment shows that the decrease of the effective rigidity is a collective property due to nonlocal effects, which cannot be explained by treating the membrane as an assembly of independent patches. This is evident from the behavior of a single inclusion, which does not lead to an asymptotic decrease of the effective rigidity; it is the combined interplay of all inclusions distributed over the whole membrane that lowers the rigidity at a specific location.

The formula (35) also holds for the modulated phases in the asymptotic limit $\hat{\xi}_{\|} \gg 1$, as checked by explicit calculations. There are additional corrections which are more complex than the one in (34) and decay as $\sim 1/\hat{\xi}_{\|}^4$.

In the aggregated phase, and as long as the domain size of the condensed inclusions is much larger than the in-plane correlation length $\xi_{\|}$, the average roughness is simply given by a weighted average of (25) with the bending rigidities κ_0 for the pure membrane and $\kappa_0 + \delta\kappa$ for the condensed domains, leading to

$$\frac{1}{\kappa_{eff}} = \left(\frac{1-\phi}{\sqrt{\kappa_0}} + \frac{\phi}{\sqrt{\kappa_0 + \delta\kappa}} \right)^2 . \tag{36}$$

The effective rigidity is increased as compared to the result (35) for the disordered and modulated phases. This corresponds to a decrease of the free energy and thus reflects the trend to aggregation on a more phenomenological level. (This approach will be expounded in the last section.)

3. Annealed versus quenched averaging

For the disordered phase the natural question arises whether a coupling of the distribution of inclusions, $\delta\kappa(\mathbf{x})$, to the membrane shape, i.e., calculating an annealed average over $\delta\kappa(\mathbf{x})$, leads to an additional contribution to the effective rigidity as given by (34). In fact, the annealed average of the effective roughness $\langle l^2\rangle$ for a random distribution $\delta\kappa(\mathbf{x})$ defined by its moments (11) and (13) turns out to be

$$\begin{aligned}\langle l^2\rangle^{D,an} &= \langle l^2\rangle^{D,qu} + \frac{1}{A4T^2}\int_{\mathbf{xyz}}\left[\overline{\delta\kappa(\mathbf{y})\delta\kappa(\mathbf{z})} - \overline{\delta\kappa(\mathbf{y})}\ \overline{\delta\kappa(\mathbf{z})}\right]\langle l(\mathbf{x})^2[\nabla^2 l(\mathbf{y})]^2\rangle_0^c\langle[\nabla^2 l(\mathbf{z})]^2\rangle_0 \\ &= \langle l^2\rangle^{D,qu} + \langle l^2\rangle_0\frac{\delta\kappa^2}{4\kappa_0^2}(\phi-\phi^2)(1-1/4\hat{\xi}_\parallel^2)\ , \end{aligned} \tag{37}$$

where $\langle l^2\rangle^{D,qu}$ denotes the result (33) obtained for quenched averaging; the two different averages differ by a correction term which does not vanish in the asymptotic limit. To understand this correction better, we calculate the density of inclusions for both averages. In the quenched case, one obviously obtains

$$\langle\phi(\mathbf{x})\rangle^{D,qu} \equiv \int_{\mathbf{x}}\langle\delta\kappa(\mathbf{x})\rangle^{D,qu}/A\delta\kappa = \phi. \tag{38}$$

For the annealed case, however, one gets

$$\begin{aligned}\langle\phi(\mathbf{x})\rangle^{D,an} &= \phi - \frac{1}{2AT\delta\kappa}\int_{\mathbf{xy}}\Big[\overline{\delta\kappa(\mathbf{x})\delta\kappa(\mathbf{y})} \\ &\quad -\overline{\delta\kappa(\mathbf{x})}\ \overline{\delta\kappa(\mathbf{y})}\Big]\langle[\nabla^2 l(\mathbf{y})]^2\rangle_0 \\ &= \phi - \frac{\delta\kappa}{2\kappa_0}(\phi-\phi^2)(1-1/4\hat{\xi}_\parallel^2)\end{aligned} \tag{39}$$

with a decreased area fraction due to the unfavorable coupling of the stiff inclusions to the fluctuating membrane (for $\delta\kappa > 0$). Now inserting (39) into (33) one clearly generates the correction term present in (37); conversely, the difference in the effective roughness between the annealed and the quenched case vanishes if the effective area fraction is identical. It follows that the coupling of the positions of the inclusions to the membrane shape does not yield a softening of the membrane, contrary to what one might intuitively guess. The same result is found for the spontaneous-curvature inhomogeneities considered in the next section.

B. Spontaneous-curvature inhomogeneity

1. Single inclusion

The calculation is analogous to the one for the rigidity coupling. In contrast, the first order contribution vanishes, and the roughness at a position $\mathbf{x}$ relative to the inclusion located at $\mathbf{x}_1 = \mathbf{0}$ is given by

$$\langle l(\mathbf{x})^2\rangle = \langle l^2\rangle_0 + \frac{a^4\kappa_0^2\delta c_1}{T^2}[C_\nabla^{(2)}(\mathbf{x})]^2, \tag{40}$$

leading to

$$\langle l(\mathbf{0})^2\rangle = \langle l^2\rangle_0\left\{1+\frac{4\kappa_0\delta c_1^2 a^4}{T\hat{\xi}_\parallel^2}\left[\ln(\hat{\xi}_\parallel^4/4+1)\right]^2\right\} \tag{41}$$

for $\mathbf{x} = \mathbf{0}$ and to

$$\langle l(\mathbf{x})^2\rangle = \langle l^2\rangle_0\left\{1+\frac{4\kappa_0\delta c_1^2 a^4}{T\hat{\xi}_\parallel^2}\left[\ker(\sqrt{2}x/\xi_\parallel)\right]^2\right\} \tag{42}$$

for $\mathbf{x} \neq \mathbf{0}$. A region of increased (or decreased) spontaneous curvature locally always increases the roughness, but as for the rigidity coupling this influence vanishes in the asymptotic limit.

2. Extended phases

For an inhomogeneous distribution $\delta c(\mathbf{x})$ of spontaneous curvature the spatially averaged roughness is given by

$$\begin{aligned}\langle l^2\rangle = \langle l^2\rangle_0 &- \frac{\kappa_0}{AT}\int_{\mathbf{xy}}\overline{\delta c(\mathbf{y})}\langle l(\mathbf{x})^2\nabla^2 l(\mathbf{y})\rangle_0^c \\ &+\frac{\kappa_0^2}{A2T^2}\int_{\mathbf{xyz}}\overline{\delta c(\mathbf{y})\delta c(\mathbf{z})}\langle l(\mathbf{x})^2\nabla^2 l(\mathbf{y})\nabla^2 l(\mathbf{z})\rangle_0^c\ .\end{aligned} \tag{43}$$

For homogeneous coverage with inclusions, defined by $\delta c(\mathbf{x}) = \delta c$, the contribution due to the perturbation vanishes and one has $\langle l^2\rangle^C = \langle l^2\rangle_0$. This can be seen already from the bare Hamiltonian (1), where the constant spontaneous curvature c_0 does not influence the membrane behavior since the integral over the curvature over the planar membrane is a constant. For the disordered phase, defined by (12) and (14), the resultant roughness is

$$\langle l^2\rangle^D = \langle l^2\rangle_0 + \frac{(\phi-\phi^2)\delta c^2\kappa_0^2 a^2}{T^2}\int_{\mathbf{q}} \mathbf{q}^4\left[G^{(2)}(\mathbf{q})\right]^2$$
$$= \langle l^2\rangle_0\left\{1+(\phi-\phi^2)\frac{\delta c^2 a^2\kappa_0}{2T}\right\}. \quad (44)$$

By comparison with (26), the effective rigidity is given by

$$\kappa_{eff} = \kappa_0\left\{1-(\phi-\phi^2)\frac{\delta c^2 a^2\kappa_0}{T}\right\}. \quad (45)$$

This can be transformed into a form which had been deduced from the hat model previously [25]:

$$\frac{1}{\kappa_{eff}} = \frac{1}{\kappa_0} + \frac{\phi(1-\phi)\delta c^2 a^2}{T}. \quad (46)$$

In contrast to the results for the rigidity coupling, the effective rigidity now depends on the type of modulated order even in the asymptotic limit. The roughness for the stripe, chessboard, and hexagonal phases, which were defined in Sec. III, is given by

$$\langle l^2\rangle^S = \langle l^2\rangle_0 + \frac{\phi\delta c^2\kappa_0^2}{4T^2}\left(Q^4[G^{(2)}(Q)]^2 + a^2\int_{\mathbf{q}}\mathbf{q}^4\left[G^{(2)}(\mathbf{q})\right]^2\right), \quad (47)$$

$$\langle l^2\rangle^C = \langle l^2\rangle_0 + \frac{\phi\delta c^2\kappa_0^2}{8T^2}\left(Q^4[G^{(2)}(Q)]^2 + 3a^2\int_{\mathbf{q}}\mathbf{q}^4\left[G^{(2)}(\mathbf{q})\right]^2\right), \quad (48)$$

$$\langle l^2\rangle^H = \langle l^2\rangle_0 + \frac{3\phi\delta c^2\kappa_0^2}{8T^2}\left(Q^4[G^{(2)}(Q)]^2 + a^2\int_{\mathbf{q}}\mathbf{q}^4\left[G^{(2)}(\mathbf{q})\right]^2\right), \quad (49)$$

with $\phi = 1/2$, $\phi = 1/2$, and $\phi = 1/4$, respectively. In the asymptotic limit, as $\xi_\parallel \to \infty$, the effective rigidity for the three different modulated phases is given by (46) with the factor $(1-\phi)$ being replaced by $1/4$, $3/8$, and $3/8$, for the striped ($\phi = 1/2$), chessboard ($\phi = 1/2$), and hexagonal phases ($\phi = 1/4$), respectively. One sees that the effective rigidity of the modulated phases is always lower than the one of the disordered phase at the corresponding coverage ϕ.

V. MONTE CARLO SIMULATIONS

In order to check the results of the perturbation calculation we performed Monte Carlo simulations for the case of symmetric inclusions. In the simulations, we used a more realistic potential containing a hard wall given by

$$V(l) = \begin{cases} \infty & \text{for } l \le 0 \\ Pl & \text{for } 0 \le l, \end{cases} \quad (50)$$

as relevant for membranes on a substrate or membranes in a stack which experience an external pressure [31]. The hard wall takes into account that membranes cannot penetrate the substrate or a neighboring membrane. Experimentally, a pressure can be applied by various means, including mechanical, osmotic, and vapor-pressure techniques [32]. For membranes with constrained solvent fraction [33] the pressure plays the role of a Lagrange multiplier fixing the separation between membranes [34]. There is good evidence that for a potential given by (50) the different separation coordinates in a stack actually decouple, so that the behavior of a stack should not differ from the behavior of a single separation coordinate [35], unlike the case for a stack which is held together by short-ranged attractive forces between the individual membranes [36]. For the simulations, the Hamiltonian (1) is discretized on a square lattice with lattice constant $a_\parallel$ [37].

A. Aggregation of inclusions

In the first part of the simulations we investigate the aggregation of inclusions based on the mechanism expounded in Sec. III. The parameters of the unperturbed membrane are $a_\parallel = 1$ and $\kappa_0/T = 1/4$. The mean separation $\ell \equiv \langle l\rangle$ is accurately described by

$$\ell \approx \left(\frac{2c_{Fl}T^2}{\kappa P}\right)^{1/3}, \quad (51)$$

which follows from a minimization of the free-energy density $f = P\ell + V_{Fl}(\ell)$. The fluctuation potential $V_{Fl}(\ell)$ is given by $V_{Fl}(\ell) = c_{Fl}T^2/\kappa\ell^2$ with the coefficient determined as $c_{Fl} = 0.116 \pm 0.002$ [35]; the elastic constant κ appearing in (51) is the bending rigidity of an individual membrane in a pair of identical membranes, which is related to the bending rigidity κ_0 of the separation coordinate by $\kappa = 2\kappa_0$ [16]. For the pressure potential with a hard wall defined by (50), the parallel correlation length $\xi_\parallel$ is related to the mean separation ℓ via $\xi_\parallel = 8(\kappa/T)^{1/2}\ell/\mathcal{C}_\parallel$ with $\mathcal{C}_\parallel \simeq 5.8319$ [19]. In Fig. 5 we show three instantaneous configurations of inclusions in a membrane, which are described by the Hamiltonian (2) with the parameters given by (a) $P/T = 0.01$ leading to $\hat{\xi}_\parallel \equiv \xi_\parallel/a_\parallel = 2.767$, (b) $P/T = 0.1$ and $\hat{\xi}_\parallel = 1.284$, and (c) $P/T = 1.0$ and $\hat{\xi}_\parallel = 0.596$. In the simulation, the positions of the inclusions and the membrane configuration were updated separately, allowing the inclusions to move to neighboring sites only; the snapshots in Fig. 5 were taken after the system had been equilibrated for 10^6 Monte Carlo steps starting with a random initial configuration. For all three simulations, the ratio of the inclusion rigidity and the membrane rigidity was taken to be $(\kappa_0+\delta\kappa)/\kappa_0 = 2000$, the spontaneous curvature of the inclusions was zero, and the linear size of a protein was fixed at $a/a_\parallel = 2$. The area fraction was set at $\phi = 1/2$. Clearly, the inclusions in Fig. 5(b) form a condensed phase which is phase separated from a phase almost free of inclusions. In Fig. 5(c) some clustering

is visible, whereas in Fig. 5(a) no correlations between the inclusions are detectable. The parameter values of these simulations are denoted in Fig. 3 by filled circles. There is qualitative agreement with the results of the perturbation theory in that only the simulation for an intermediate value of $\hat{\xi}_{\|}$ shows aggregation; the effective value of $\hat{S}$ of the simulations thus lies somewhere between $\hat{S} \approx 0.2$ and ≈ 0.5. To literally connect the perturbation parameter $\hat{S}$ with the parameters of the simulations would be illusory, due to the many approximations made in the analytic calculation. One issue which could not be addressed in the theory is the size of an inclusion. The simulations indeed demonstrate that the effective parameter $\hat{S}$ scales inversely proportional with the relative inclusion size $a/a_{\|}$, as speculated in Sec. III: For $a/a_{\|} = 1$ no aggregation could be observed for any parameters [38], while for $a/a_{\|} = 3$ the aggregated phase persists to much smaller values of the pressure P/T.

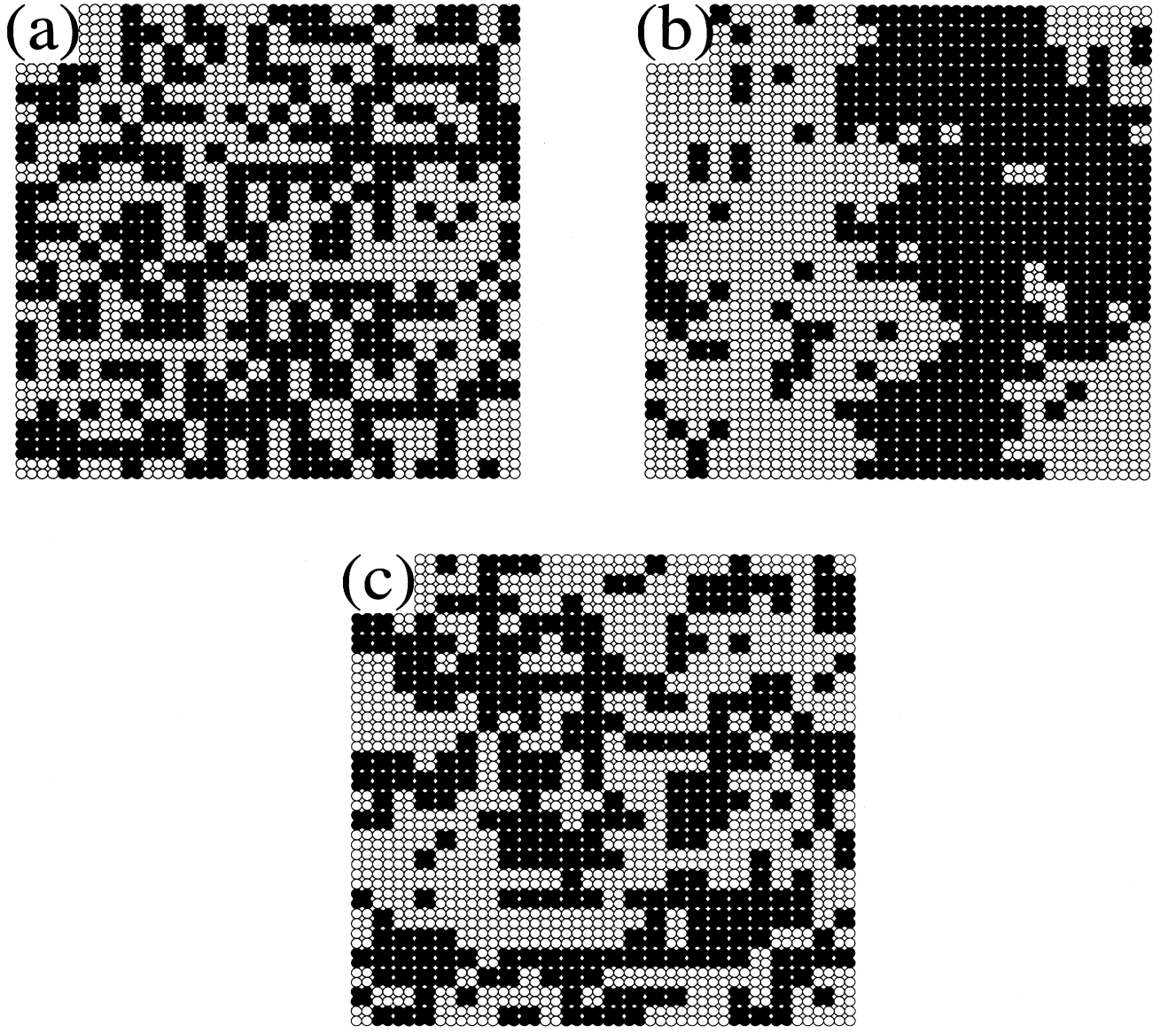

FIG. 5. Configurations of inclusions or proteins with linear size a after equilibration for 10^6 Monte Carlo steps at three different pressures: (a) $P = 0.01$ ($\hat{\xi}_{\|} = 2.767$), (b) $P = 0.1$ ($\hat{\xi}_{\|} = 1.284$), and (c) $P = 1.0$ ($\hat{\xi}_{\|} = 0.596$). Each protein covers four lattice sites of the underlying lipid matrix with lattice constant $a_{\|}$. There is strong aggregation leading to a single domain of clustered proteins for the intermediate value of the pressure, in agreement with the phase diagram in Fig. 3.

B. Effective bending rigidity

We also studied the behavior of the effective bending rigidity κ_{eff}. For the presentation of our data, we introduce the dimensionless height variable $z \equiv l\sqrt{2\overline{\kappa}/T}/a_{\|}$ and the rescaled pressure $p \equiv P/a_{\|}^3/\sqrt{2\overline{\kappa}T}$, where the mean bending rigidity $\overline{\kappa}$ is given by the arithmetic average $\overline{\kappa} = (1-\phi)\kappa_0 + \phi(\kappa_0 + \delta\kappa)$. We performed four series of simulations for different values of $\delta\kappa/\kappa_0$, namely, $\delta\kappa/\kappa_0 = 0$, 2, 6, and 18, with a fixed area fraction $\phi = 1/2$. In Fig. 6 we plot the ratios of $\langle z\rangle$ for $\delta\kappa/\kappa_0 \neq 0$ and $\delta\kappa/\kappa_0 = 0$. For the data denoted by open circles, the inclusions could not diffuse and were distributed according to a chessboard pattern with the lattice constant identical to the underlying discretization lattice. By plotting the ratio, we isolate the softening effect due to fluctuations: if the effective bending rigidity κ_{eff} was given by the mean bending rigidity $\overline{\kappa}$, all three data sets would coincide. In fact, the Monte Carlo data saturate at values different from unity as the pressure decreases. In order to obtain good statistics, we had to sample over 10^7 Monte Carlo steps, using lattices with up to 3600 sites; the resulting statistical errors are denoted by vertical bars. Calculating the mean separation ℓ for $\delta\kappa/\kappa_0 \neq 0$ by substituting $\kappa = 2\kappa_{eff}$ as given by (35) into the expression (51), and the mean separation for $\delta\kappa/\kappa_0 = 0$ by substituting $\kappa = 2\kappa_0$ into (51), and using $\langle z\rangle = \ell\sqrt{2\overline{\kappa}/T}/a_{\|}$, the ratio turns out to be given by

$$\frac{\langle z(\delta\kappa/\kappa_0)\rangle}{\langle z(\delta\kappa/\kappa_0 = 0)\rangle} = \left(\frac{(1+\phi\delta\kappa/\kappa_0)[1+(1-\phi)\delta\kappa/\kappa_0]}{1+\delta\kappa/\kappa_0}\right)^{1/3}. \quad (52)$$

This prediction, which should be valid asymptotically for vanishing pressure, is denoted by horizontal broken lines in Fig. 6 for the three different values of $\delta\kappa/\kappa_0$ used; there is good agreement with the Monte Carlo results for small enough pressure. We also did some simulations for freely diffusing inclusions where the same parameters were used as for the chessboard configurations. The closed circles denote simulations in the canonical ensemble with a fixed number of inclusions on the lattice (with $\phi = 1/2$), and the open squares denote simulations in the grand canonical ensemble, where the thermal average of the density is fixed at $\phi = 1/2$ by application of a suitably chosen chemical potential. The numerical effort is much higher, since an additional local degree of freedom, namely, the position of the inclusions, has to be equilibrated in addition to the membrane shape. For the specific parameters used, the inclusions are disordered and far from forming an aggregated phase. The data are very close to the data for the chessboard pattern, denoted by open circles. This agrees with the prediction from Sec. IV A that a disordered and a modulated distribution of inclusions should have the same effective rigidity for $\xi_{\|} \gg a_{\|}$ and that annealing the inclusion distribution at fixed density does not lead to an additional softening of the membrane.

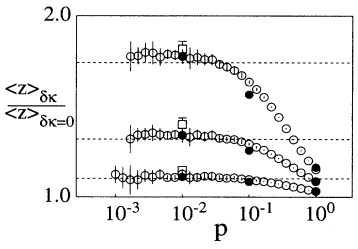

FIG. 6. Ratio of $\langle z(\kappa/\kappa_0 \neq 0)\rangle$ over $\langle z(\kappa/\kappa_0 = 0)\rangle$ for three different values of $\delta\kappa/\kappa_0$, namely, $\delta\kappa/\kappa_0 = 2$, 6, and 18, at an area fraction $\phi = 1/2$. Open circles denote results for a fixed chessboard configuration of the inclusions, closed circles for a fixed number of freely diffusing inclusions, and open squares for freely diffusing inclusions in the grand canonical ensemble. Note that inclusions are disordered for the parameter values considered here. The broken lines denote the predictions of the perturbation theory; the numerical uncertainties are given by the vertical error bars.

VI. CONCLUSIONS

In summary, we performed a perturbation calculation for inhomogeneous fluid membranes in the effective perturbation parameters $\delta\kappa/\kappa_0$ and $\delta c a\sqrt{\kappa_0/T}$ where $\delta\kappa$ and δc are the excess rigidity and spontaneous curvature of inclusions immersed in the otherwise homogeneous membrane. The effects described in this article arise due to a coupling of thermally activated shape fluctuations to the lateral distribution of inclusions. The free energy and the effective bending rigidity κ_{eff} of different phases were calculated up to second order in the effective perturbation parameters. The resulting phase diagram features the disordered phase, where inclusions are randomly distributed, the aggregated phase, where the mixed system separates into a phase of close-packed inclusions and the pure membrane without inclusions, and various modulated phases in the case where the spontaneous curvatures of the inclusions all have the same sign. A single-mode description was used for the modulated phases. We checked the predictions for symmetric inclusions by lattice Monte Carlo simulations using a potential which takes into account the impenetrability of neighboring molecules.

The phase behavior can be understood based on the interaction between two single inclusions, which are for the following arguments supposed to be stiffer than the surrounding membrane and have spontaneous curvatures of the same sign. Then the shape fluctuations of the membrane lead to an attraction due to the rigidity coupling and to a repulsion due to the curvature coupling between the inclusions. The latter interaction prefers modulated phases, the former leads to aggregation. The control parameter turns out to be the in-plane correlation length

$\xi_\parallel$ of the membrane, which measures the decay of lateral height-height correlations. This parameter can be experimentally controlled in various ways. In vesicle experiments, $\xi_\parallel$ depends on material parameters but also on the pressure difference between the inside and the outside of the vesicle, which in turn can be easily changed by osmotic techniques. Also, binding a vesicle to a substrate changes the pressure due to concomitant shape transformations but also influences the correlations directly in the part of the membrane which is exposed to the binding substrate [39]. In experiments on oriented stacks of membranes, the correlation length $\xi_\parallel$ is proportional to the mean separation between the membranes, which is above the critical unbinding transition simply determined by the solvent fraction. Changing $\xi_\parallel$ corresponds to a path on a straight line passing through the origin in the phase diagrams in Fig. 2. The slope of this line depends on the characteristics of the inclusion considered, namely, on the ratio of the bending rigidity and the spontaneous curvature induced in the membrane. Causing the aggregation transition or the formation of hexagonal order by changing the correlation length $\xi_\parallel$ also rules out competing mechanisms (as described in the Introduction) as an explanation for the phase change, since these should not depend on $\xi_\parallel$.

Finally, we would like to discuss the aggregation transition of a membrane with an area fraction ϕ of inclusions on a more phenomenological basis using the concept of the effective bending rigidity κ_{eff}. For concreteness, we will use the picture of a stack of membranes at a fixed mean separation ℓ between nearest-neighboring membranes. Neglecting attractive interactions which are small for the case where a stack can be swollen indefinitely, the main contribution to the free energy is the fluctuation interaction $V_{Fl}(\ell)$; see Sec. V. In the disordered phase, where the inclusions are randomly mixed, the free energy (neglecting translational entropy of the proteins) is in the asymptotic limit and using (35) given by

$$f \sim \frac{T^2}{\kappa_{eff}\ell^2} \simeq \frac{T^2}{\ell^2}\left(\frac{1-\phi}{\kappa_0}+\frac{\phi}{\kappa_0+\delta\kappa}\right), \tag{53}$$

where κ_0 is the bending rigidity of the pure membrane and $\kappa_0+\delta\kappa$ is the bending rigidity of an inclusion. In the aggregated phase, there is a macroscopic phase separation in each relative displacement field in the stack into patches free of inclusions with bending rigidity κ_0 and a mean separation ℓ_0 and patches of close-packed inclusions controlled by a bending rigidity $\kappa_0+\delta\kappa$ with a mean separation ℓ_δ. The free energy is now given by a weighted average of the fluctuation interaction $V_{Fl}(\ell)$ over all patches and reads

$$f \sim T^2\left(\frac{1-\phi}{\kappa_0\ell_0^2}+\frac{\phi}{(\kappa_0+\delta\kappa)\ell_\delta^2}\right). \tag{54}$$

This expression has to be minimized in accord with the conserved-volume constraint $\ell=(1-\phi)\ell_0+\phi\ell_\delta$, which ensures that the mean separation averaged over the patches in the whole system is still given by ℓ. The result of the minimization is

$$f \sim \frac{T^2}{\ell^2}\left(\frac{1-\phi}{\kappa_0^{1/3}}+\frac{\phi}{(\kappa_0+\delta\kappa)^{1/3}}\right)^3, \tag{55}$$

which is for all values of the parameters involved lower than (53) [40]. This difference of the free energies is the driving mechanism for the stabilization of the aggregated phase. The perturbation calculation, taking into account the finite correlation length $\xi_\parallel$ and the translational entropy of the inclusion, yields the more refined phase diagram given in Fig. 2. Note that for the modulated phases the heuristic free energy written as in (53) has to be supplemented by a contribution from the coupling between the spontaneous curvature of the inclusions and the actual curvature of the membrane, which is of the form $\langle\delta c(\mathbf{x})\nabla^2 l(\mathbf{x})\rangle$. An interesting result of the above treatment is the prediction of two coexisting mean separations ℓ_0 and ℓ_δ in a stack of membranes hosting the aggregated protein phase, which might be observable using x-ray scattering techniques. The two separations are related by $\ell_0/\ell_\delta = 2(1-\tau^{1/3}+\tau^{2/3})/(1+\tau)$ with $\tau=\phi\kappa_0/(1+\phi)(\kappa_0+\delta\kappa)$. In fact, since the clustering of proteins occurs in the separation coordinate between neighboring membranes, this aggregation has the tendency to propagate vertically from one membrane pair to the adjacent one. The mean separation for membranes covered with inclusions is smaller than for membranes free of inclusions, so a vertical correlation of protein clusters leads to strains in the stack. These strains are relieved by introducing domains of stagger-stacked protein patches, which raises the free energy due to the presence of domain boundaries [41].

ACKNOWLEDGMENTS

R.R.N. is indebted to R. Lipowsky for introduction into the subject and for many helpful comments. It is a pleasure to thank M. Goulian, C. Jeppesen, D. Morse, K.M. Palmer, J. Rädler, and C.R. Safinya for enjoyable and useful discussions. This work was supported by the MRL Program of the National Science Foundation under Awards No. DMR-9123048 and No. DMR-9301199. R.R.N. acknowledges receipt of a NATO science stipend administered by the DAAD.

APPENDIX A: CORRELATION FUNCTIONS

The correlation functions needed in the text are defined by

$$C^{(2)}_{\nabla^2}(\mathbf{x}_1-\mathbf{x}_2) \equiv \langle\nabla^2 l(\mathbf{x}_1)\nabla^2 l(\mathbf{x}_2)\rangle_0^c = \int_{\mathbf{q}} \mathbf{q}^4 e^{i\mathbf{q}\cdot(\mathbf{x}_1-\mathbf{x}_2)} G^{(2)}(\mathbf{q}) , \tag{A1}$$

$$C^{(4)}_{\nabla^2}(\mathbf{x}_1-\mathbf{x}_2) \equiv \langle[\nabla^2 l(\mathbf{x}_1)]^2[\nabla^2 l(\mathbf{x}_2)]^2\rangle_0^c = \int_{\mathbf{q}} e^{i\mathbf{q}\cdot(\mathbf{x}_1-\mathbf{x}_2)} G^{(4)}_{\nabla^2}(\mathbf{q}) , \tag{A2}$$

$$C_{\nabla}^{(2)}(\mathbf{x}_1-\mathbf{x}_2) \equiv \langle \nabla l(\mathbf{x}_1)\nabla l(\mathbf{x}_2)\rangle_0^c = \int_{\mathbf{q}} \mathbf{q}^2 e^{i\mathbf{q}\cdot(\mathbf{x}_1-\mathbf{x}_2)} G^{(2)}(\mathbf{q}) \ , \quad \text{(A3)}$$

where $\int_{\mathbf{q}} \equiv \int d^2\mathbf{q}/(2\pi)^2$. These correlation functions can be calculated exactly for the Hamiltonian defined by (1) if one chooses a harmonic potential, given by

$$V(l) = (m/2)l^2. \quad \text{(A4)}$$

Then, the propagators appearing in (A1)–(A3) are given by

$$G^{(2)}(\mathbf{q}) = \frac{T}{\kappa_0 \mathbf{q}^4 + m} \ , \quad \text{(A5)}$$

$$G^{(4)}_{\nabla^2}(\mathbf{q}) = 2\int_{\mathbf{p}} (\mathbf{p}+\mathbf{q})^4 G^{(2)}(\mathbf{p}+\mathbf{q})\mathbf{p}^4 G^{(2)}(\mathbf{p}) \ , \quad \text{(A6)}$$

leading to the closed-form expressions [13]

$$C^{(2)}_{\nabla^2}(|\mathbf{x}_1-\mathbf{x}_2|) = \frac{T}{\pi\kappa_0\xi_\parallel^2}\mathrm{kei}(\sqrt{2}|\mathbf{x}_1-\mathbf{x}_2|/\xi_\parallel) \ , \quad \text{(A7)}$$

$$C^{(4)}_{\nabla^2}(|\mathbf{x}_1-\mathbf{x}_2|) = \frac{2T^2}{\pi^2\kappa_0^2\xi_\parallel^4}[\mathrm{kei}(\sqrt{2}|\mathbf{x}_1-\mathbf{x}_2|/\xi_\parallel)]^2 \ , \quad \text{(A8)}$$

$$C^{(2)}_{\nabla}(|\mathbf{x}_1-\mathbf{x}_2|) = \frac{T}{2\pi\kappa_0}\mathrm{ker}(\sqrt{2}|\mathbf{x}_1-\mathbf{x}_2|/\xi_\parallel) \quad \text{(A9)}$$

for $\mathbf{x}_1 \neq \mathbf{x}_2$, where the correlation length is defined by

$$\xi_\parallel = (4\kappa_0/m)^{1/4}. \quad \text{(A10)}$$

The function $G^{(4)}_{\nabla^2}(\mathbf{q})$ is calculated in Appendix C. For large arguments, the Thomson functions exhibit oscillatory behavior with an exponentially decaying envelope and are given by [43]

$$\mathrm{ker}(x) \simeq \sqrt{\frac{\pi}{2x}} e^{-x/\sqrt{2}} \cos(-z/\sqrt{2}-\pi/8) \ , \quad \text{(A11)}$$

$$\mathrm{kei}(x) \simeq \sqrt{\frac{\pi}{2x}} e^{-x/\sqrt{2}} \sin(-z/\sqrt{2}-\pi/8). \quad \text{(A12)}$$

For vanishing argument x, $\mathrm{ker}(x)$ is positive and diverges, whereas $\mathrm{kei}(0) = -\pi/4$.

APPENDIX B: INTEGRALS

Some of the integrals needed in the text diverge at the upper cutoff, which thus has to be finite and is defined by the relation $\int_{\mathbf{q}} 1 \equiv 1/a^2$. The integrals then are given by

$$\int_{\mathbf{q}} \mathbf{q}^4 G^{(2)}(\mathbf{q}) = \frac{T}{\kappa_0 a^2}\left(1-\frac{a^2}{4\xi_\parallel^2}\right) \ , \quad \text{(B1)}$$

$$\int_{\mathbf{q}} \mathbf{q}^4 \left[G^{(2)}(\mathbf{q})\right]^2 = \frac{T^2}{\kappa_0^2}\frac{\xi_\parallel^2}{32} \ , \quad \text{(B2)}$$

$$\int_{\mathbf{q}} \mathbf{q}^8 \left[G^{(2)}(\mathbf{q})\right]^2 = \frac{T^2}{\kappa_0^2 a^2}\left(1-\frac{3a^2}{8\xi_\parallel^2}\right) \ , \quad \text{(B3)}$$

$$\int_{\mathbf{q}} \mathbf{q}^8 \left[G^{(2)}(\mathbf{q})\right]^3 = \frac{T^3}{\kappa_0^3}\frac{3\xi_\parallel^2}{128} \ , \quad \text{(B4)}$$

$$\int_{\mathbf{q}} \mathbf{q}^2 G^{(2)}(\mathbf{q}) \simeq \frac{T}{2\kappa_0}\ln\left(1+\hat{\xi}_\parallel^4/4\right). \quad \text{(B5)}$$

APPENDIX C: FOUR-POINT PROPAGATOR

In this section we determine the $\mathbf{q}$-dependent part of the four-point propagator $G^{(4)}_{\nabla^2}(\mathbf{q})$. To that end, we define the function

$$G^{(4)}(\mathbf{q}) \equiv 2\int_{\mathbf{p}} G^{(2)}(\mathbf{p}+\mathbf{q})G^{(2)}(\mathbf{p}) \equiv \frac{T^2\xi_\parallel^6}{64\kappa_0^2}K(\tilde{q}), \quad \text{(C1)}$$

where $\tilde{\mathbf{q}} = \mathbf{q}\xi_\parallel/\sqrt{2}$ and $\tilde{q} = |\tilde{\mathbf{q}}|$. The auxiliary function $K(\tilde{q})$ is given by

$$\begin{aligned} K(\tilde{q}) &= \frac{4}{\pi^2}\int d^2\tilde{\mathbf{p}} \frac{1}{\tilde{\mathbf{p}}^4+1}\frac{1}{[\tilde{\mathbf{p}}+\tilde{\mathbf{q}}]^4+1} \\ &= -\frac{1}{\pi^2}\int d^2\tilde{\mathbf{p}}\left(\frac{1}{\tilde{\mathbf{p}}^2-i}-\frac{1}{\tilde{\mathbf{p}}^2+i}\right) \\ &\quad \times\left(\frac{1}{[\tilde{\mathbf{p}}+\tilde{\mathbf{q}}]^2-i}-\frac{1}{[\tilde{\mathbf{p}}+\tilde{\mathbf{q}}]^2+i}\right) \\ &= -\frac{1}{\pi^2}\left(\mathcal{I}_1+\mathcal{I}_2-\mathcal{I}_3-\mathcal{I}_4\right). \end{aligned} \quad \text{(C2)}$$

The four product integrals can be solved using the Feynman reparametrization technique defined by the equality

$$\frac{1}{AB} = \int_0^1 \frac{d\alpha}{[\alpha(A-B)+B]^2}. \quad \text{(C3)}$$

Applying this trick to the first integral yields

$$\begin{aligned} \mathcal{I}_1 &= \int d^2\tilde{\mathbf{p}} \frac{1}{(\tilde{\mathbf{p}}^2-i)([\tilde{\mathbf{p}}+\tilde{\mathbf{q}}]^2-i)} \\ &= \int_0^1 d\alpha \int d^2\tilde{\mathbf{p}} \frac{1}{\{[\tilde{\mathbf{p}}+\alpha\tilde{\mathbf{q}}]^2-i+\alpha\tilde{\mathbf{q}}^2(1-\alpha)\}^2}. \end{aligned} \quad \text{(C4)}$$

The origin of the $\tilde{\mathbf{p}}$ integration can be shifted since there is no cutoff involved and the result is

$$\mathcal{I}_1 = \frac{\pi}{\tilde{q}^2}\int_0^1 \frac{d\alpha}{\alpha(1-\alpha)-i/\tilde{q}^2} \ . \quad \text{(C5)}$$

The remaining integral is elementary and gives

$$\mathcal{I}_1 = \frac{2\pi}{\tilde{q}^2}\left(\frac{\ln(\sqrt{1-4i/\tilde{q}^2}+1)-\ln(\sqrt{1-4i/\tilde{q}^2}-1)}{\sqrt{1-4i/\tilde{q}^2}}\right). \tag{C6}$$

The analogous results for the other product integrals are

$$\mathcal{I}_2 = \int d^2\tilde{\mathbf{p}}\frac{1}{(\tilde{\mathbf{p}}^2+i)([\tilde{\mathbf{p}}+\tilde{\mathbf{q}}]^2+i)}$$

$$= \frac{\pi}{\tilde{q}^2}\int_0^1 \frac{d\alpha}{\alpha(1-\alpha)+i/\tilde{q}^2}$$

$$= \frac{2\pi}{\tilde{q}^2}\left(\frac{\ln(\sqrt{1+4i/\tilde{q}^2}+1)-\ln(\sqrt{1+4i/\tilde{q}^2}-1)}{\sqrt{1+4i/\tilde{q}^2}}\right), \tag{C7}$$

$$\mathcal{I}_3 = \int d^2\tilde{\mathbf{p}}\frac{1}{(\tilde{\mathbf{p}}^2-i)([\tilde{\mathbf{p}}+\tilde{\mathbf{q}}]^2+i)}$$

$$= \frac{\pi}{\tilde{q}^2}\int_0^1 \frac{d\alpha}{\alpha(1-\alpha)+(2\alpha-1)i/\tilde{q}^2}$$

$$= \frac{\pi}{\tilde{q}^2}\left(\frac{\ln(1+\sqrt{1-4/\tilde{q}^4})-\ln(1-\sqrt{1-4/\tilde{q}^4})}{\sqrt{1-4/\tilde{q}^4}}\right), \tag{C8}$$

$$\mathcal{I}_4 = \int d^2\tilde{\mathbf{p}}\frac{1}{(\tilde{\mathbf{p}}^2+i)([\tilde{\mathbf{p}}+\tilde{\mathbf{q}}]^2-i)}$$

$$= \frac{\pi}{\tilde{q}^2}\int_0^1 \frac{d\alpha}{\alpha(1-\alpha)-(2\alpha-1)i/\tilde{q}^2}$$

$$= \frac{\pi}{\tilde{q}^2}\left(\frac{\ln(1+\sqrt{1-4/\tilde{q}^4})-\ln(1-\sqrt{1-4/\tilde{q}^4})}{\sqrt{1-4/\tilde{q}^4}}\right). \tag{C9}$$

After some algebraic manipulation one arrives at the result

$$K(\tilde{q}) = \frac{4}{\pi\tilde{q}^2}\left\{\frac{\operatorname{arctanh}(1-4/\tilde{q}^4)^{1/2}}{(1-4/\tilde{q}^4)^{1/2}} - \frac{(\sqrt{1+16/\tilde{q}^4}+1)^{1/2}\operatorname{arctanh}(\sqrt{1/4+4/\tilde{q}^4}+1/2)^{-1/2} - (\sqrt{1+16/\tilde{q}^4}-1)^{1/2}\arctan(\sqrt{1/4+4/\tilde{q}^4}-1/2)^{-1/2}}{(2+32/\tilde{q}^4)^{1/2}}\right\}. \tag{C10}$$

The limiting behavior of $K(\tilde{q})$ for $\tilde{q} \ll 1$ and $\tilde{q} \gg 1$ can be combined into

$$K(\tilde{q}) \sim \frac{4}{\tilde{q}^4+4}. \tag{C11}$$

Finally, the $\mathbf{q}$-dependent part of $G^{(4)}_{\nabla^2}(\mathbf{q})$ is given by $G^{(4)}_{\nabla^2}(\mathbf{q}) = 16G^{(4)}(\mathbf{q})/\xi_\parallel^8$ so that we obtain

$$G^{(4)}_{\nabla^2}(\mathbf{q}) = \frac{T^2}{4\kappa_0^2\xi_\parallel^2}K(\tilde{q}). \tag{C12}$$

[1] E. Sackmann, R. Kotulla, and F.-J. Heiszler, Can. J. Biochem. Cell Biol. **62**, 778 (1984).
[2] B.A. Lewis and D.M. Engelman, J. Mol. Biol. **166**, 203 (1983).
[3] L.T. Pearson, J. Edelman, and S.I. Chan, Biophys. J. **45**, 863 (1984).
[4] R. Blankenburg, P. Meller, H. Ringsdorf, and C. Salesse, Biochemistry **28**, 8214 (1989).
[5] B. Sternberg, A. Watts, and Z. Cejka, J. Struct. Biol. **110**, 196 (1993).
[6] S. Marčelja, Biochim. Biophys. Acta **455**, 1 (1976).
[7] H. Schröder, J. Chem. Phys. **67**, 1617 (1977).
[8] J.C. Owicki, M.W. Springgate, and H.M. McConnell, Proc. Natl. Acad. Sci. USA **75**, 1616 (1978); J.C. Owicki and H.M. McConnell, *ibid.* **76**, 4750 (1979).
[9] F. Jähnig, Biophys. J. **36**, 329 (1981).
[10] O.G. Mouritsen and M. Bloom, Biophys. J. **46**, 141 (1984).
[11] N. Dan, P. Pincus, and S.A. Safran, Langmuir **9**, 2768 (1993).
[12] M. Goulian, R. Bruinsma, and P. Pincus, Europhys. Lett. **22**, 145 (1993); **23**, 155 (1993).
[13] K.M. Palmer, M. Goulian, and P. Pincus, J. Phys. (France) II **4**, 805 (1994).
[14] R. Bruinsma, M. Goulian, and P. Pincus, Biophys. J. **67**, 746 (1994).
[15] For recent reviews, see *Statistical Mechanics of Membranes and Surfaces*, edited by D. Nelson, T. Piran, and S. Weinberg (World Scientific, Singapore, 1989); *The Structure and Dynamics of Membranes*, edited by R. Lipowsky and E. Sackmann, Handbook on Biological Physics Vol. 1 (Elsevier, Amsterdam, 1995).

[16] For the case of two membranes, the effective rigidity κ_0 is a function of the bending rigidities of the two individual membranes, κ_1 and κ_2, and is given by $\kappa_0 = \kappa_1\kappa_2/(\kappa_1 + \kappa_2)$.
[17] See, for example, J. Goos and G. Gompper, J. Phys. (France) I **3**, 1551 (1993).
[18] H. Gruler, Z. Naturforsch. Teil C **30**, 608 (1975).
[19] R.R. Netz, Phys. Rev. E **51**, 2286 (1995).
[20] The free energy can also be calculated for annealed disorder, thereby taking into account correlations between inclusions; however, it is *a priori* not clear whether this improves the quality of the resultant phase diagram, since the entropy as given in (15) is based on the random-mixing approximation corresponding to an uncorrelated distribution of inclusions. In fact, for simple lattice models, the two errors of neglecting correlations in the energetic and in the entropic contributions usually compensate each other to a large degree, and taking correlations into account for only one contribution typically does not lead to better results as compared to exact solutions.
[21] S. Leibler, J. Phys. (Paris) **47**, 507 (1986).
[22] S. Leibler and D. Andelman, J. Phys. (Paris) **48**, 2013 (1987).
[23] A.N. Berker and J.S. Walker, Phys. Rev. Lett. **47**, 1469 (1981); R.R. Netz and A.N. Berker, *ibid.* **68**, 333 (1992); in *Phase Transitions in Liquid Crystals*, edited by S. Martellucci and A.N. Chester (Plenum, New York, 1992), p. 109; A.N. Berker, J.O. Indekeu, and R.R. Netz, Turk. J. Phys. **18**, 358 (1994).
[24] The effective rigidity of a mixed membrane has been estimated very recently using the hat model, which assumes different patches of the membrane to be fluctuating independently governed by local effective rigidities given by a simple superposition of the bare rigidity κ_0 and the perturbation $\delta\kappa$ [25,26]. The present calculation shows that this picture is inaccurate on a microscopic level.
[25] W. Helfrich and M.M. Kozlov, J. Phys. (France) II **4**, 1427 (1994).
[26] W. Helfrich, Liq. Cryst. **5**, 1647 (1989).
[27] If one bends a membrane with an inhomogeneous bending modulus without fixing the shape in detail, the resulting profile will minimize the total bending energy by concentrating the elastic deformations at locations of reduced bending modulus; this effect also leads to an elastic softening even at zero temperature which, in contrast to the fluctuation effect discussed in the present work, strongly depends on the spatial distribution of the rigidity inhomogeneities.
[28] V.S. Markin, Biophys. J. **36**, 1 (1981).
[29] S.T. Milner and T.A. Witten, J. Phys. (Paris) **49**, 1951 (1988).
[30] J.T. Brooks, C.M. Marques, and M.E. Cates, Europhys. Lett. **14**, 713 (1991).
[31] We also did Monte Carlo simulations using a harmonic potential and trivially reproduced the analytic predictions for small enough interaction parameters.
[32] See, e.g., V.A. Parsegian, N. Fuller, and R.P. Rand, Proc. Natl. Acad. Sci. USA **76**, 2750 (1979); R.P. Rand and V.A. Parsegian, Biochim. Biophys. Acta **988**, 351 (1989).
[33] F.C. Larche, J. Appell, G. Porte, P. Bassereau, and J. Marignan, Phys. Rev. Lett. **56**, 1700 (1986); J. Appell, P. Bassereau, J. Marignan, and G. Porte, Colloid Polym. Sci. **267**, 600 (1989); C.R. Safinya, D. Roux, G.S. Smith, S.K. Sinha, P. Dimon, N.A. Clark, and A.M. Bellocq, Phys. Rev. Lett. **57**, 2718 (1986).
[34] S. Leibler and R. Lipowsky, Phys. Rev. B **35**, 7004 (1987).
[35] R.R. Netz and R. Lipowsky, Europhys. Lett. **29**, 345 (1995).
[36] R.R. Netz and R. Lipowsky, Phys. Rev. Lett. **71**, 3596 (1993).
[37] R. Lipowsky and B. Zielinska, Phys. Rev. Lett. **62**, 1572 (1989).
[38] The maximal relative rigidity of the inclusions which can be simulated effectively is given by $\delta\kappa/\kappa_0 \approx 10^5$; above, the diffusion of inclusions is very slow and the equilibration times become prohibitively long.
[39] J.O. Rädler, T.J. Feder, H.H. Strey, and E. Sackmann, Phys. Rev. E **51**, 4526 (1995).
[40] The result (55) can also be derived similarly to the arguments which led to (36). Inserting (51) into the free-energy expression $f = P\ell + V_{Fl}(\ell)$ one obtains $f \sim (2c_{Fl}T^2P^2/\kappa)^{1/3}$. In the segregated phase, one has the condensed regions with bending rigidity $\kappa_0 + \delta\kappa$ and regions without inclusions with κ_0; the weighted average is $f \sim (2c_{Fl}T^2P^2/\kappa_{eff})^{1/3}$ with the effective rigidity $\kappa_{eff} = [(1-\phi)/\kappa_0^{1/3} + \phi/(\kappa_0 + \delta\kappa)^{1/3}]^3$ which via (51) is identical to (55). The difference between the above expression for κ_{eff} and (36) is due to the presence of the hard wall in the first case.
[41] These domain boundaries are positioned both perpendicular and parallel to the membrane normal, thus leading to a situation where the separations of neighboring membrane pairs are unequal; in this case the quasi-separability mentioned in Sec. V breaks down. The effective free energy for a separation coordinate can be written in a form analogous to (53) with a modified effective bending rigidity now also depending on the relative separations of the neighboring membranes [42]; the resultant changes in the free energy are rather small and only contribute to the interfacial energy of these domain boundaries.
[42] R.R. Netz, Phys. Rev. E **52**, 1897 (1995).
[43] *Handbook of Mathematical Functions*, edited by M. Abramowitz and I.A. Stegun (Dover Publications, New York, 1972); I.S. Gradshteyn and I.M. Ryzhik, *Table of Integrals, Series, and Products* (Academic Press, New York, 1980).